Helium ion beam induced growth of hammerhead AFM probes

Gaurav Nanda[a)]
Kavli Institute of Nanoscience, Delft University of Technology, Lorentzweg 1, 2628 CJ Delft, The Netherlands

Emile van Veldhoven and Diederik Maas
TNO Science and Industry, Stieltjesweg 1, 2628 CK Delft, The Netherlands

Hamed Sadeghian
TNO Science and Industry, Stieltjesweg 1, 2628 CK Delft, The Netherlands and Department of Precision and Microsystems Engineering, Delft University of Technology, 2628 CJ Delft, The Netherlands

Paul F. A. Alkemade[b)]
Kavli Institute of Nanoscience, Delft University of Technology, Lorentzweg 1, 2628 CJ Delft, The Netherlands

(Received 27 June 2015; accepted 6 November 2015; published 18 November 2015)

The authors report the direct-write growth of hammerhead atomic force microscope (AFM) probes by He^+ beam induced deposition of platinum-carbon. In order to grow a thin nanoneedle on top of a conventional AFM probe, the authors move a focused He^+ beam during exposure to a PtC precursor gas. In the final growth stage, a perpendicular movement of the beam results in the required three-dimensional (hammerhead) shape. The diameter of the needle depends on the ion beam dose, beam dwell time, and speed of the beam movement. A nanoneedle radius below 10 nm and a hammerhead smaller than 35 nm have been achieved. This fabrication process is robust and enables precise control over the three-dimensions of the hammerhead AFM probe. Finally, the authors test the capabilities of the fabricated AFM probes for two-dimensional metrology of sidewall angles and line-edge roughness of trenches and shark-fins in silicon. © *2015 American Vacuum Society*.
[http://dx.doi.org/10.1116/1.4936068]

I. INTRODUCTION

The atomic force microscope (AFM) is increasingly being used for high precision profiling and metrology in semiconductor processing, such as for the measurement of roughness and height of trenches made in photoresist. However, measurements of undercut, sidewall roughness, and critical dimensions (CD) have not yet been optimized in accordance with the International Technology Roadmap for Semiconductors (ITRS) recommendations.[1] A limiting factor is the extension of the probe–resist interaction region when the tip of an AFM probe is inserted into a trench. The conventional conical or parabolic-shaped AFM tip is incapable of resolving undercuts and sidewall roughness due to the lack of access of the tip to these features of the trenches.

In order to improve the probe–surface interaction and, hence, to truly resolve 3D structures, a 3D-AFM probe is needed. For a CD measurement, the tip must have a lateral protrusion in order to measure the sidewalls and angles with sufficient accuracy.[2,3] The first demonstration of such a probe was reported by Martin and Wickramasinghe[2] for CD measurements, where a 3D-AFM with a hammerhead or boot tip shape is scanned in CD mode and in deep-trench mode. Later, these 3D probes have been applied for the critical dimension metrology by Dixson *et al.*[3,4] and Foucher *et al.*[5,6] However, still lacking is a one-step fabrication method to grow such probes with high reproducibility. Various attempts have been made to grow or to shrink the size of these probes by electron beam induced deposition (EBID) followed by plasma etching.[5–7] However, EBID with a stationary electron beam usually gives relatively thick needles due to the scattering of primary and secondary electrons (SEs) in the growing material.[8] One way to minimize the scattering is to use a horizontal growth mode, i.e., using a horizontally moving beam during EBID. This mode usually results in needles of around 18–100 nm in diameter.[9] In this work, we use a focused He^+ beam to make a 3D probe with a hammerhead tip. The main advantage of a He^+ beam is that the interacting volume of the helium ions is smaller than that for an electron beam or a gallium focused ion beam (Ga-FIB) at the same acceleration voltage.[10] Because of the small interaction volume, the helium ion microscope has been used as a nanofabrication tool in recent years, e.g., for the modification of graphene,[11,12] for lithography,[13] and for ion beam induced deposition (IBID).[14] Using a stationary He^+ beam, Chen *et al.*[8] fabricated 36-nm wide PtC pillars. Moreover, we expect the dimensions to be even smaller when using the horizontal growth mode. Therefore, the aim of our present work is to explore the use of He^+ IBID in the horizontal growth mode for making high-aspect 3D-AFM probes.

II. EXPERIMENTAL SECTION

The experiments are performed in a Carl Zeiss Orion™ Plus scanning helium ion microscope, equipped with an omniGIS system from Omniprobe. A nozzle with a 500-μm wide opening is positioned around 150-200 μm above the sample during the deposition. The nozzle is at an angle of

a)Electronic mail: g.nanda@tudelft.nl
b)Electronic mail: p.f.a.alkemade@tudelft.nl

25° to the surface normal. The working distance is 9.2 mm. The precursor gas $(CH_3)_3Pt(C_PCH_3)$ is used, mixed with N_2 carrier gas in the ratio of 1:10. The background pressure in the microscope is around 5×10^{-7} mbar, rising to 8×10^{-6} mbar during deposition. Tapping-mode silicon AFM probes from NanoAndMore Gmbh are used as the base material. There is a possibility that during the AFM measurement the grown needle breaks or buckles,[9] leading to unintentional scanning with the standard AFM probe. To eliminate this possibility, we cut the top of the conventional silicon AFM probe using Ga-FIB milling [see Fig. 1(b)]. Thereafter, the AFM probe is cleaned gently with acetone and isopropanol and then mounted vertically in the helium ion microscope such that the truncated probe of the cantilever is perpendicular to the incident beam. The He^+ beam is aimed onto the edge of the cantilever and then slowly moved horizontally away from the edge into the vacuum, such that a continuous needle-like structure grows; see the schematic of this process in Fig. 1(a). Next, the beam is moved in the perpendicular horizontal direction to form two lateral protrusions. The exposure of the very end of the tip to the helium ions should be minimized to avoid sputtering of silicon. Therefore, we start with focusing the beam at the edge of the cantilever and then we move the beam slowly toward the tip. Before the actual growth, we perform a test deposition nearby to make sure the beam conditions are optimal. We performed plasma cleaning of the chamber before loading the sample. After cleaning, we performed several deposition tests without the precursor gas and did not observe any deposition. We used an Elphy Plus (Raith GmbH) pattern generator, 1-nm beam step size, and a beam current below 1 pA. The Raith pattern generator is programmed such that the nanoneedle is grown in one continuous process. The current is set by regulating the helium gas pressure in the source. In order to optimize the growth of freestanding nanoneedles, we varied the beam dwell time between 1 and 20 ms. The grown nanoneedles are imaged by subsequent helium ion microscope (HIM) imaging with a 0.3 pA beam current. To test the hammerhead AFM probes, 2D AFM scans are carried out using a Bruker FastScan AFM system on trenches made in silicon. These trenches are made by e-beam lithography and chlorine-based reactive ion etching.

III. RESULTS AND DISCUSSION

For the nanoneedle growth, 30-keV beam energy and 0.35 ± 0.05 pA current are used. For a step size of 1 nm, the flux is 1.25×10^{20} ions cm^{-2} s^{-1}.

Figure 1(b) shows the cutting of the standard AFM probe by Ga-FIB milling, followed by the successive growth of the hammerhead nanoneedle by He-IBID [Fig. 1(c)]. Figure 2 shows HIM images of nanoneedles grown on the edge of the truncated silicon cantilever. The beam is moved from left to right [Figs. 2(a)–2(d)], extending beyond the edge of the silicon. We found that below the critical dose of 5×10^{17} ions cm^{-2}, no horizontal growth beyond the edge took place ($l = 0$). Apparently, the dwell time is then too short to complete 1-nm (i.e., the step size) growth at the apex, see (1, 2) in Fig. 2(c). At 5×10^{17} ions cm^{-2}, a thin needle of ~14 nm in diameter extending from the edge into the vacuum is obtained. The apex of the growing needle is supplied with precursor molecules via direct adsorption and via surface diffusion from the substrate edge.[15] Due to the increasing distance, the diffusion of precursor molecules from the substrate edge decreases, and, hence, needles become thinner near the apex [see Figs. 2(c)–2(d)]. Apparently, the amount of deposited material progressively reduces while the horizontal beam shift proceeds.[16] At some point, the beam shift outruns the precursor supply and the growth stops. As a result, the final needle is shorter than designed ($l < L$); see (3) in Fig. 2(c). Thus, at short dwell times, nanoneedles are short and have very sharp ends. The observed behavior suggests that the horizontal growth is influenced by the transition from an ion-limited growth mode to a precursor-limited growth mode.[15] For dwell times of 6 ms and longer, nanoneedles are grown with the desired length ($l = L$); see (4) in Fig. 2(c).

For increasing dose above 5×10^{17} ions cm^{-2}, the nanoneedles thicken (see Fig. 3). They reach a diameter of 62 nm at 2.5×10^{18} ions cm^{-2}. Smith *et al.*,[17] Chen *et al.*,[8] and Fujita *et al.*[18] have demonstrated that for a stationary ion beam the vertical growth is dominated by the decomposition of precursor molecules by primary ions and SEs. The initial nanoneedle is widened by the forward scattered ions that exit the vertical needle from the side. In contrast, our moving

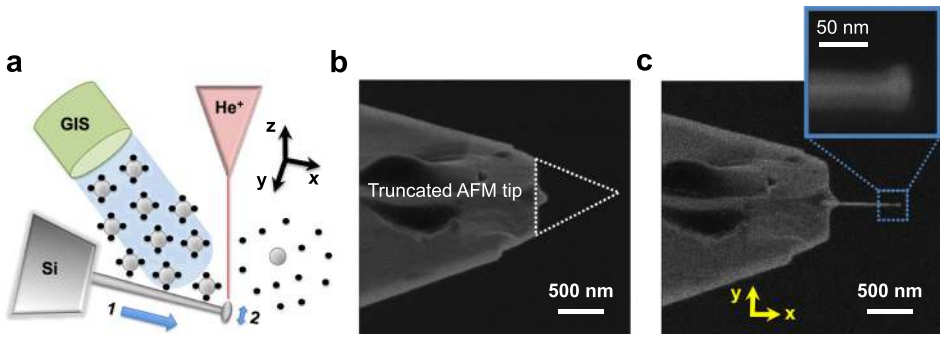

FIG. 1. (Color online) Fabrication of a PtC AFM probe with a hammerhead using $(CH_3)_3Pt(C_PCH_3)$ precursor decomposition with a focused He^+ beam at 0.3 pA and 30 keV. (a) Sketch of the last step of the hammerhead growth. In the presence of the precursor gas, the beam is slowly moved from left to right (1); in the last step, the beam is moved in the perpendicular direction (2). HIM images of the growth; (b) Original AFM probe with removed apex before tip growth, where dotted lines show the removed part; (c) The same probe after growth of the nanoneedle with a hammerhead shape (inset shows the hammerhead).

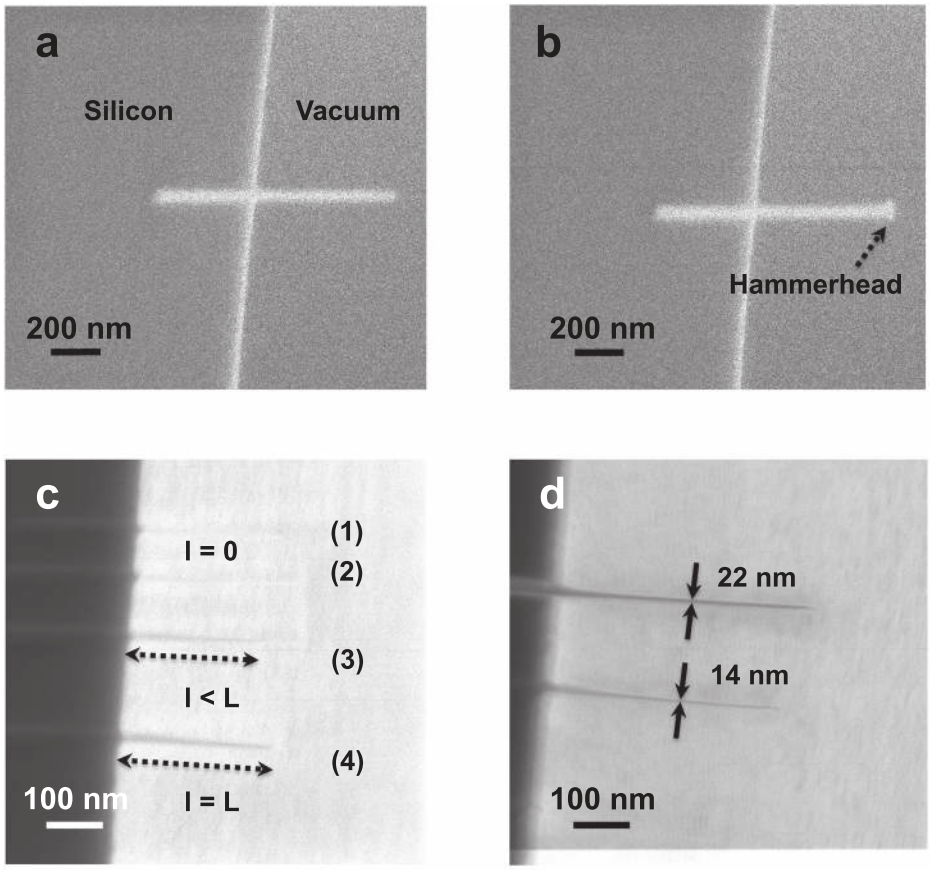

FIG. 2. HIM images of nanoneedles grown by He-IBID, where l is the grown length and L is the designed length of the nanoneedle. (a) Nanoneedle grown beyond the edge of a silicon sample via the horizontal growth mode; (b) needles with a 3D hammerhead grown at the apex via the perpendicular growth mode; (c) growth for various dwell times for a fixed current; (1, 2) no growth, here the dwell time was too short to form a free-standing needle, (3) precursor-limited growth, here the grown needle is shorter than the designed length, and (4) successful growth, where the needle has the designed length; (d) two needles, grown with different dwell times.

helium ion beam passes through the apex of the growing horizontal nanoneedle. As a consequence, the nanoneedles remain much thinner.

Figure 3 shows the needle diameter as a function of the dwell time or dose. With the increase in dose, we obtain a thicker needle. The deposition efficiency (V_{ion}), i.e., the needle volume per incident ion, is given by

$$V_{\text{ion}} = \frac{\pi D^2 s e}{4 \tau_{\text{dwell}} i}, \tag{1}$$

where D is the needle diameter, s is the beam step size (1 nm in our experiment), i is the beam current, and τ_{dwell} is the dwell time. The deposition efficiency V_{ion} is 0.03 nm^3 ion^{-1}, comparable to 0.04 nm^3 ion^{-1} for the stationary He^+ beam at the same current, although at a lower beam energy of 25 keV.[8] Three regimes can be distinguished in the plot of the needle volume per ion versus dwell time: (1) the nucleation regime (0–4 ms in Fig. 3) where no significant growth takes place; (2) an intermediate regime (4–8 ms) characterized by a fast increase of the needle volume per ion; (3) and the saturation regime (beyond 12 ms) where the needle volume per ion attains a more or less constant value. The primary helium beam traverses the tip apex and generates SEs, which are emitted from a volume larger than the beam diameter. The SEs dissociate adsorbed molecules, and, hence, material is being deposited.[15] The mean free path (or escape distance) of the SEs and the geometrical spreading of the SE flux determine the diameter of the growing material. If the dwell time τ_{dwell} is increased, more SEs are being generated

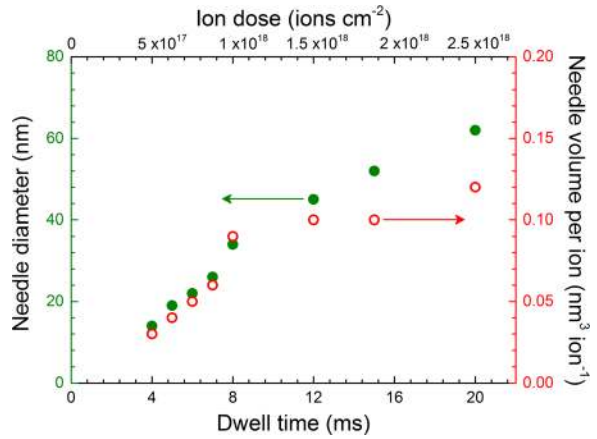

FIG. 3. (Color online) Nanoneedle diameter at half-length as a function of dwell time or ion dose. No needles did grow at dwell times less than 4 ms. Red open circles show the deposition efficiency as a function of beam dwell time.

and a larger volume is grown. Obviously, the growth in the x-direction during τ_{dwell} must be equal to the beam step size of 1 nm. The additional volume growth for increased dwell times is, thus, in the y- and z-directions. If the needle width becomes larger than the mean free path of the SEs (a few nanometers[15,17]), the broadening in the y-direction saturates.

Assuming a density of 11 PtC_4 molecules nm^{-3},[8] ~3 molecules are decomposed per ion for the thinnest needle, most likely by SEs generated by the primary beam.[8,15] Figure 4(a) shows a 13-nm nanoneedle grown on a truncated conventional AFM probe. The depositions were started ~200 nm from the edge [see Fig. 4(a)]. The figure demonstrates that the process with the moving He^+ ion beam enables us to fabricate needles with a diameter down to 13 nm and a length up to ~700 nm. Needles have been grown on various days under slightly varying conditions. In all attempts, we reduced the dwell time slowly until no or a too-short needle appeared. We have made at least ten series of needles on the edges of a silicon sample and on the truncated AFM tips with currents ranging from 0.3 to 0.6 pA. We observed that the diameter of the narrowest successful hammerhead needle was always 13–14 nm, independent of the actual current. This procedure to produce hammerhead AFM probes is, thus, robust. Figure 4(b) shows HIM images of hammerhead tips grown with slightly different final beam movements; see the yellow insets. Single spot exposure [lower left in Fig. 4(b)] gives a spherical head because of the higher number of isotropically emitted SEs. When the beam is moved in the +y-direction [upper right in Fig. 4(b)], an elliptical or hook-like shape is obtained. Two small protrusions are grown by moving the beam in the +y and −y directions [upper left and lower right in Fig. 4(b)], giving the needle a hammerhead shape. Schematics of these movements are shown by the insets in Fig. 4(b).

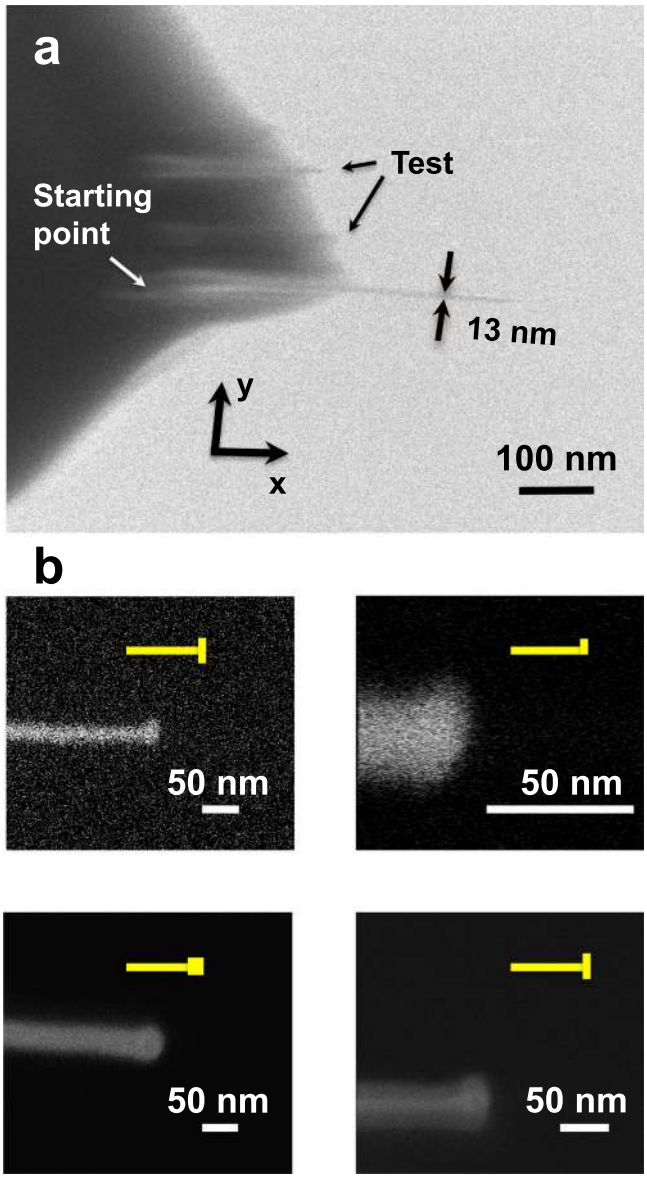

FIG. 4. (Color online) (a) Nanoneedle grown on the gallium FIB modified AFM probe. Two test needles are grown before the actual needle growth to ensure the focus and beam conditions are optimal; (b) tips grown with various beam movements, as shown in the insets.

The ions of the helium beam do not only contribute to needle growth via precursor decomposition, but also to needle break-down by sputtering. However, the sputtering yield for He^+ ions is low, typically less than 0.1 atoms ion^{-1}.[19] Hence, the net growth yield is mainly determined by precursor decomposition, in contrast to growth via heavy-ion beam induced deposition.[20,21]

Finally, 2D AFM measurements are carried out to illustrate the usefulness of the hammerhead probe. For this purpose, trenches in silicon with varying pitch and shark-fin sample structures are measured. Figures 5(a) and 5(b) show AFM images of the trenches. The measured depth of the silicon trenches in Figs. 5(b) and 5(c) is ~75 nm, in good agreement with the designed depth of 75 ± 5 nm using plasma etching. Discrepancies in the measured profile are most likely due to redeposited particles on the trench bottom and tilting over of the trench edges; whereas the V-shape is either due to partial isotropy in the etching or to the needle shape. These AFM measurements are taken with an AFM probe with a 35-nm hammerhead. Fine details are observable along the trench sidewalls, and some particles can be seen on the trench bottom; see the dotted circle in Fig. 5(b). Thus, we conclude that the hammerhead probe is effective and can resolve small geometrical features. For comparison Fig. 5(d) shows a HIM image of similar trenches but with a slightly different pitch. Figure 5(e) shows AFM images of the shark-fin sample. Interestingly, the 35-nm hammerhead probe can resolve the sharp apex of the shark-fin [see Figs. 5(e) and 5(f)]. The measured tip angle of the shark-fin is ~33°, in good agreement with the nominal value of ~30°. The nominal height of the shark-fin is ~300 nm. Each tip is used for several AFM measurements over a period of at least 1 month. We have not observed any variation in the obtained morphology of the trenches or any buckling. This reproducibility demonstrates the probe's stability during deep-trench measurements. We note that the scanning system of our standard 2D-AFM is only capable of measuring the tip's z motion. Therefore, it is not possible to scan the vertical trench edges; for that purpose one needs a 3D-AFM. Full characterization of these probes could include stiffness and

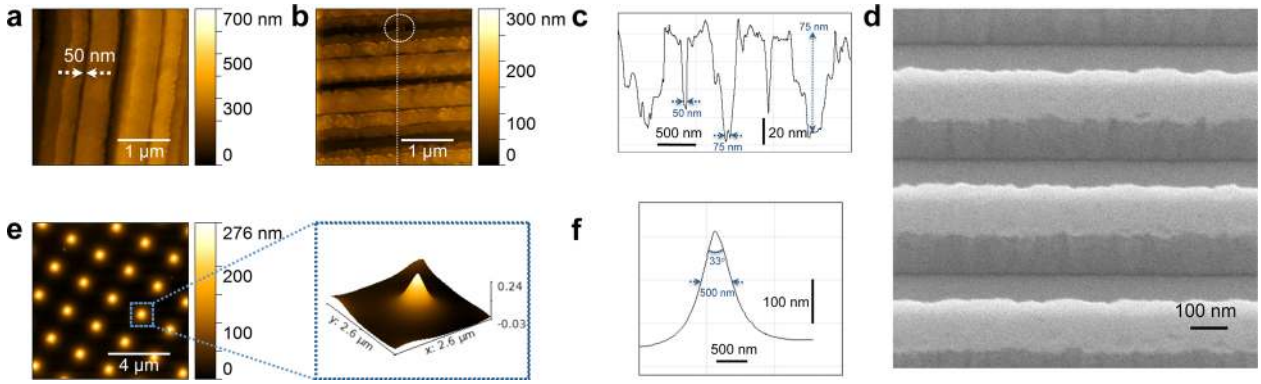

FIG. 5. (Color online) (a) and (b) AFM images of trenches in silicon obtained with 35-nm hammerhead probes. Sidewall roughness are clearly seen along the trenches; (c) the profile along the dotted line of the structure in (b); (d) HIM image of the trenches in silicon (the sample is 40° tilted); (e) 2D-scan of a shark-fin sample; (f) the line profile across the shark-fin.

stability tests during AFM scanning and TEM study of the thickness (i.e., in the z-direction) of the probes, the length of the overhang, and the radius of the hammerhead edges, all as function of the growth conditions.

IV. CONCLUSION

Silicon-based AFM probes suffer from strong limitations with regard to tip width, length, and shape to fulfill ITRS recommendations for 3D CD metrology. In this paper, we have investigated the capabilities of He^+ beam processing (He-IBID) for the growth of thin needles with hammerhead tips as probes for 3D AFM measurements. The He-IBID grown probes have distinct merits because of their high aspect ratio and the possibility for relatively easy customization. The lateral movement of the ion beam during growth determines the 3D probe shape. This one-step process enables precise control over the tip shape and length. We have grown PtC 3D-AFM probes with a minimum diameter of 13 nm and with 35-nm wide hammerheads. The main factors that enable the small width of our nanoneedles are the subnanometer ion-beam size, the negligible scattering of primary and secondary particles, negligible ion-beam sputtering, and a balance between the beam movement speed and the needle growth rate. Our 2D AFM measurements show that the probes can be used for AFM measurements without any noticeable wear. We conclude that this one-step He-IBID process to grow 3D AFM probes is an important step toward meeting the requirements of CD metrology.

ACKNOWLEDGMENTS

The authors thank the Dutch Technology Foundation STW, which is part of The Netherlands Organization for Scientific Research (NWO), and the Ministry of Economic Affairs for funding this research. The authors thank Rodolf Herfst, Maarten van Es, and Sasan Aliasghar Keyvani (all from TNO Delft) for their help with the AFM measurements.

[1]G. Dai, M. Heidelmann, C. Kübel, R. Prang, J. Fluegge, and H. Bosse, Meas. Sci. Technol. **24**, 085001 (2013).
[2]Y. Martin and H. K. Wickramasinghe, Appl. Phys. Lett. **64**, 2498 (1994).
[3]R. Dixson and A. Guerry, SPIE Proc. **5375**, 633 (2004).
[4]R. Dixson, N. G. Orji, J. Fu, M. Cresswell, R. Allen, and W. Guthrie, SPIE Proc. **6152**, 61520P–1 (2006).
[5]J. Foucher, E. Pargon, M. Martin, S. Reyne, and C. Dupré, SPIE Proc. **6922**, 69220F (2008).
[6]J. Foucher, P. Filippov, C. Penzkofer, B. Irmer, and S. W. Schmidt, SPIE Proc. **8681**, 86811I (2013).
[7]M. Wendel, H. Lorenz, and J. P. Kotthaus, Appl. Phys. Lett. **67**, 3732 (1995).
[8]P. Chen, E. van Veldhoven, C. A. Sanford, H. W. M. Salemink, D. J. Maas, D. A. Smith, P. D. Rack, and P. F. A. Alkemade, Nanotechnology **21**, 455302 (2010).
[9]J. D. Beard and S. N. Gordeev, Nanotechnology **22**, 175303 (2011).
[10]D. C. Bell, M. C. Lemme, L. A. Stern, and C. M. Marcus, J. Vac. Sci. Technol. B **27**, 2755 (2009).
[11]N. Kalhor, S. A. Boden, and H. Mizuta, Microelectron. Eng. **114**, 70 (2014).
[12]G. Nanda, S. Goswami, K. Watanabe, T. Taniguchi, and P. F. A. Alkemade, Nano Lett. **15**, 4006 (2015).
[13]V. Sidorkin, E. van Veldhoven, E. van der Drift, P. Alkemade, H. Salemink, and D. Maas, J. Vac. Sci. Technol. B **27**, L18 (2009).
[14]P. F. A. Alkemade, E. M. Koster, E. van Veldhoven, and D. J. Maas, Scanning **34**, 90 (2012).
[15]P. F. A. Alkemade, P. Chen, E. van Veldhoven, and D. Maas, J. Vac. Sci. Technol. B **28**, C6F22 (2010).
[16]G. C. Gazzadi, S. Frabboni, and C. Menozzi, Nanotechnology **18**, 445709 (2007).
[17]D. A. Smith, D. C. Joy, and P. D. Rack, Nanotechnology **21**, 175302 (2010).
[18]J. Fujita, M. Ishida, T. Ichihashi, Y. Ochiai, T. Kaito, and S. Matsui, J. Vac. Sci. Technol. B **21**, 2990 (2003).
[19]M. Stepanova and S. Dew, *Nanofabrication* (Springer-Verlag, Wien, 2012) p. 279.
[20]Y. H. Kahng *et al.*, Ultramicroscopy **110**, 82 (2009).
[21]A. D. Dubner and A. Wagner, J. Appl. Phys. **66**, 870 (1989).